Characterization of gradient properties generated by SMAT for a biomedical grade 316L stainless steel

Yangcan Wu, Bruno Guelorget, Zhidan Sun, Régis Deturche, Delphine Retraint

Characterization of gradient properties generated by SMAT for a biomedical grade 316L stainless steel

Y. Wu[1], B. Guelorget[1], Z. Sun[1], R. Déturche[2], D. Retraint[1*]

[1]ICD, P2MN, LASMIS, University of technology of Troyes, CNRS FRE 2019, Troyes, France
[2]ICD, P2MN, L2n, University of technology of Troyes, CNRS FRE 2019, Troyes, France

[*]Corresponding author: Delphine RETRAINT, delphine.retraint@utt.fr, Tel.: +33-3-25-71-56-68

Abstract

Gradient microstructure generated by SMAT (Surface Mechanical Attrition Treatment) has beneficial effects for treated mechanical components, such as improved fatigue behaviour and tensile yield stress. Little effort has been devoted to characterize the local properties of each region in the gradient microstructure generated by SMAT. In this paper, the gradient microstructure was first highlighted by microscopic observation using Electron Back-Scatter Diffraction (EBSD). Nanoindentation was used to characterize the loading-unloading behaviour at different depths beneath the treated surface. All the indentation patterns were observed using Atomic Force Microscopy (AFM) and a pile-up phenomenon was detected. The nanoindentation results were analysed taking into account this pile-up effect on the dimension of the imprints. The results reveal that grain refinement plays a dominant role on the hardness values, while the effect of residual stress is less significant. In addition, correcting the indentation contact area appears to be necessary in the near surface region which is strongly affected by SMAT.

Keywords: SMAT, Gradient properties, Grain refinement, Nanoindentation, Pile-up

1. Introduction

Mechanical surface treatments are increasingly used to enhance the life of engineering parts by altering the near-surface microstructure and consequently the mechanical properties of materials. These techniques, such as shot peening [1,2], deep rolling [3,4] or micro-percussion [5], are based on contact loadings and can create significant plastic deformation in the near surface region [6]. As a result, a compressive residual stress field along with a work hardened region is generated after treatment, which is generally beneficial to enhance fatigue properties of materials including crack initiation and propagation [7].

Surface Mechanical Attrition Treatment (SMAT) is one of the most promising mechanical surface treatment techniques. It is based on repetitive multi-directional impacts between the surface of a part and spherical shot boosted by an ultrasonic vibrating sonotrode [8,9]. The near surface region is mechanically affected by impact loadings. This can lead to a progressive grain size refinement due to severe plastic deformation, whereas the bulk of the part is not mechanically deformed and its characteristics as well as its mechanical properties remain unchanged. A gradient microstructure is thus formed from the treated surface to the inner region of the material [10–13]. The particularity of SMAT with respect to conventional shot peening lies in the fact that it can transform the top surface layer of materials from coarse grains to nano-sized grains [8,9]. This nanostructured layer, even if it is

generally thin [14], could have significant effect on the performance of materials, since engineering components are mostly loaded on their surface, for example in the case of friction, bending, torsion or contact loadings.

The gradient microstructure induced by SMAT can be roughly divided into three areas: the core material region which is not affected by the treatment, the transition region and the nanocrystalline layer which is located at the top surface. The beneficial effects owing to the gradient microstructure generated by SMAT have been investigated in previous studies [12, 13, 15]. Nevertheless, emphasis was mainly placed on the global properties of the gradient microstructure and little effort has been devoted to investigate the individual properties of each layer. For instance, Zhou et al. [13] investigated the influence of SMAT on fatigue behaviour of 316L stainless steel. It was concluded that the gradient microstructure enhanced the fatigue strength of the treated material. The beneficial effects of gradient microstructure have also been observed in terms of improving the tensile strength of SMAT-processed 316L stainless steel [15]. In fact, when a mechanical component is subjected to SMAT, grain refinement, superficial compressive residual stresses and strain hardening are simultaneously introduced as a result of severe plastic deformation. These three factors co-exist along the cross-section of the treated part and all vary according to the distance to the treated surface. Therefore, the enhanced properties of the gradient microstructure are due to the combined effects of these SMAT-induced parameters.

To better understand the beneficial effects of the gradient microstructure, it would be valuable to characterize the mechanical behaviour at different depths in relation to the SMAT-processed surface, such as the nanostructured layer and the mechanically deformed region. Characterization of the local mechanical behaviour of the nanostructured layer is difficult, given its very small thickness (from several microns to tens of microns, depending on the treatment intensity). In the literature, nanoindentation technique was widely used to study the local mechanical behaviour of materials at micro- or nano-scale, such as thin films [16–20] or multi-phased materials [21–23]. Hence, nanoindentation provides access to individual characterization of different layers in the gradient microstructure. The local mechanical properties of each layer could be derived according to its indentation behaviour, such as the maximum load, final displacement during unloading and residual indentation imprint [24–26]. For instance, Gale et al. [27] investigated the nanoindentation behaviour of SMAT-processed copper with varied indentation load. Their results showed that indentation behaviours, such as indentation depth and pile-up height, were different for SMAT-affected region and the bulk region.

In this work, the local mechanical behaviour of gradient microstructure of 316L stainless steel generated by SMAT was investigated using nanoindentation technique. First, the gradient microstructure of the material was highlighted using Electron BackScatter Diffraction (EBSD). Then, nanoindentation tests were performed at different distances from the treated surface. Maximum load, hardness and pile-up behaviour were studied as function of the distance beneath the treated surface. The residual indentation imprints were then observed using Atomic Force Microscopy (AFM) in order to analyse pile-up or sink-in phenomenon that could occur as a function of distance to the SMAT-processed surface. The indentation behaviour of different layers, along with EBSD and AFM observations, were analysed to interpret the local properties of the SMAT-processed material with gradient microstructure.

2. Material and experimental procedure

2.1. Material and SMAT

The material investigated in this work is a biomedical grade 316L stainless steel. Tab. 1 gives information about the chemical composition of this alloy. SMAT is based on the projection of metallic spherical shot (3 mm diameter) towards the surface of a part due to a high frequency (20 kHz) ultrasonic vibrating sonotrode. In this study, a dumbbell shape specimen was treated by SMAT. Its gauge length is 12 mm with a diameter of 6 mm. SMAT was performed so as to cover the entire gauge length of the specimen. Concerning the SMAT conditions, the specimen was subjected to a treatment of 15 minutes with a generator power of 30%, followed by a treatment of 5 minutes with a generator power of 50%.

Table 1. Chemical composition (wt.%) of the studied 316L stainless steel.

Fe	C	Mn	Si	P	S	Cr	Ni	Mo	Cu	N	Ti	V
Balance	0.013	1.7	0.26	0.017	0.003	17.37	14.52	2.80	0.08	0.088	<0.005	0.07

2.2. Microstructure observation using EBSD

EBSD was used to observe the microstructure on the cross-section of the specimen processed by SMAT. For this purpose, an EBSD sample was prepared by transversely cutting the central part of the SMAT-processed dumbbell shape specimen. This EBSD sample was then molded, mechanically ground, polished to a mirror-like finish and finally polished with an OPS solution. The EBSD observation was performed using a scanning electron microscope FEG-SEM SUPRA 55 VP operating at 20 kV equipped with the OIM™ software system.

2.3. Nanoindentation tests

The nanoindentation tests were carried out with a NanoIndenter XP^{TM} at room temperature (former MTS, now KLA-Tencor, San José, CA), fitted with a Berkovich indenter. The maximum displacement into the sample was 500 nm with a strain rate of 0.05 s^{-1} and the distance between any two neighbouring indents was at least 15 µm. This distance was chosen to avoid possible influence of stress field caused by the neighbouring indentation [28]. A number of distances ranging from 5 to 1000 µm below the treated surface were chosen in order to investigate the gradient properties.

2.4 Observation of indentation imprint using AFM

The three-dimensional shape (topography) of the residual indentation patterns were measured using an Atomic Force Microscopy (Bruker ICON). The observations were conducted in peak force mode with a silicon probe (model: scanasyst-air). For each indentation imprint, a scanning cartography of 10 µm x 10 µm was completed. The acquired data were post-treated using the software NanoScope Analysis 1.8 to detect possible pile-up or sink-in phenomenon.

3. Results and discussion

3.1 Gradient microstructure generated by SMAT

Fig. 1 shows the results of the EBSD observation performed on the cross-section of the SMAT-processed specimen. Globally, a microstructure gradient can be observed in the SMAT affected region. Three different regions can be roughly distinguished. They are respectively the nanostructured layer (the thickness of this region is thin), the SMAT unaffected inner region, and the transition region between the two previous ones. The nanostructured layer corresponds to a refined layer with a grain size ranging from 50 nm to 300 nm (Fig. 1c). This grain refinement is due to the multi-directional severe plastic deformation induced by the impingement of the flying shot [9]. According to Fig. 1c, the thickness of the nanostructured layer is about 5 µm and small grains are well formed due to high SMAT intensity. Underneath this nanostructured layer is the work hardened region. The grain size in this region varies in a larger interval (from 300 nm to several microns) [12]. As a matter of fact, the initial coarse grains are split by plastic slips activated by the multi-directional impacts of shot during SMAT and the colour (which gives information about grain orientation) in each grain is no longer uniform (Fig. 1b). New boundaries separating different coloured blocks could be detected. Hence, grain refinement occurred consequently. The extent to which these grains are refined depends on the corresponding SMAT intensity. In the bulk of the sample (far away from the treated surface), the material was not affected by SMAT because the grains do not look deformed and no plastic slip traces can be observed. In addition, a large fraction of twins can be detected in this region of the as-received state (Fig. 1a), which was probably formed during the material's initial processing. The average grain size in the inner region is about 10 µm which also corresponds to the initial grain size of the SMAT affected region. It can also be revealed that grain refinement is significant down to a depth of about 100 µm according the EBSD observations.

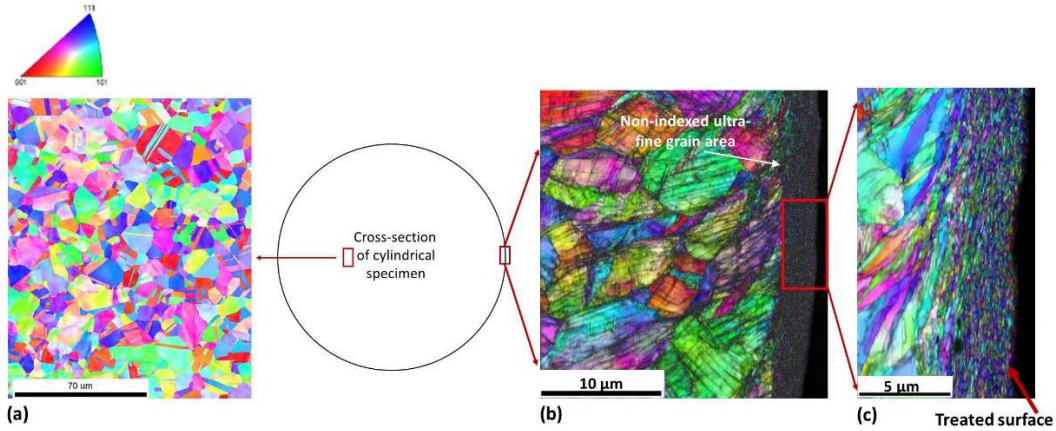

Figure 1 – Microstructure observation on the cross-section of a SMAT-processed specimen: (a) inner region (non-affected by SMAT), (b) mechanically deformed region (transition region), (c) nanostructured layer.

3.2 Gradient properties highlighted by nanoindentation

After the EBSD observations, a series of indentation tests was conducted along the cross-section of the SMAT-processed sample, and load-displacement curves were subsequently obtained. The corresponding results were plotted in Fig. 2 for different distances beneath the treated surface. A complete nanoindentation test consists of a loading part and an unloading part. Both reveal important information about the properties of the indented material, such as local strength and sign of the residual stress [24, 25, 29]. Local strength can be quantified by maximum indentation loads which are shown in Fig. 3a. The maximum load in the nanocrystalline region is about 30 mN which is

about twice higher compared to the bulk which is not affected by SMAT. The maximum indentation load is stabilized at a depth of about 550 µm below the treated surface. This indicates that the depth affected by SMAT is at least 550 µm. Three factors induced by SMAT (grain refinement, compressive residual stress and strain hardening, respectively) contribute to higher indentation load. In this work, efforts have been made to attempt to distinguish individually the influence of each of these three factors.

Firstly, it should be clarified that when SMAT intensity is high, three major changes, such as grain refinement, superficial compressive residual stress and strain hardening, are significantly induced, as compared to the non-affected region. While SMAT intensity is low and no grain refinement takes place, the material is merely slightly work hardened with limited amount of compressive residual stress. Therefore, it would be a real challenge to understand individually their roles with regard to their contributions to higher local strength in the strongly affected regions. In the literature, systematic studies were conducted to investigate the influence of residual stress on nanoindentation load [24-26, 30-32]. For example, Zhu et al. [31] performed nanoindentation (penetration depth of 700 nm) on single crystal copper with different residual stress states. The magnitude of the residual stress ranged from -137.4 MPa to 68.4 MPa. Their results showed that the influence of residual stress on indentation load is in the range of a few µN, which was negligible compared to the magnitude of the maximum load (several mN). Bolshakov et al. [26] used finite element method to study the behaviour of 8009 aluminium alloy during indentation to investigate how the indentation process was influenced by residual stress. The residual stress ranged from -300 MPa to +350 MPa for a series of simulations. The results showed that the maximum indentation load increased by about 1 mN for simulation with residual stress of -300 MPa. Similar results were found by Mady [32] for ceramic films simulated using finite element method. For a compressive residual stress of -5 GPa, the maximum load increased by only 2 mN as compared to stress-free state. In fact, when the imposed load exceeds the yield strength of the material (as it is the case during nanoindentation), residual stress has small effects because the elastic misfit strains are small and soon washed out by plasticity [33].

In our case, the studied material is a 316L stainless steel with a higher Young's modulus and hardness compared to copper and aluminium. According to our previous work, the compressive residual stress generated by SMAT is about -450 MPa in the strongly affected region [13]. Based on the above discussion, compressive residual stresses are not assumed to be a major factor which contributes to higher local strength. In the present paper, grain refinement is considered to be the main factor for higher local strength, as suggested by the Hall-Petch law. This issue will be addressed in details later in this paper (Section 3.3).

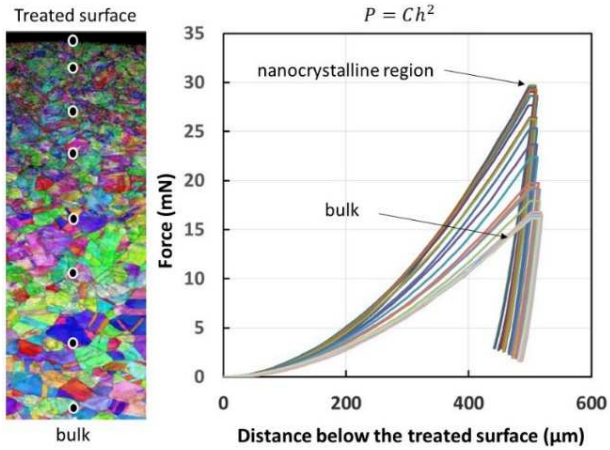

Figure 2 – Force-displacement curves of indentations at different distances below the treated surface.

Besides the loading part, the unloading curve of nanoindentation also gives important information about the indented material, such as contact stiffness and sign/magnitude of residual stress [25, 34]. For instance, the ratio between the final displacement and the maximum displacement, h_f/h_{max} could be correlated to residual stress and pile-up behaviour of the studied material [25, 29, 31, 35]. Xu et al. [29] established an empirical model based on finite element simulations for residual stress determination from the elastic recovery (h_f/h_{max}) of nanoindentation. The empirical model has been used to derive the plastic properties and to estimate the residual stress of the mechanically polished fused quartz beam. Unfortunately, this method could not be applied to our case because most of the experiments conducted in the literature do not take into account a variation of the grain size. For a SMAT-processed sample, grain size refinement induces an additional changing parameter, grain size d, which makes the interpretation of indentation measurements challenging. Hence, the ratio of h_f/h_{max} for the present experiments could not be directly correlated to superficial compressive residual stresses. The ratios of h_f/h_{max} for the indentations performed along the cross-section of the SMAT-processed sample are illustrated in Fig. 3b. It can be noticed that the elastic recovery is larger in the near treated surface while almost no elastic recovery can be found in the bulk of the sample which is not affected by SMAT. It is concluded previously that residual stresses do not have a significant influence on the load-displacement curves of nanoindentation [26, 31–33]. Therefore, the variation of elastic recovery for our experiments can be attributed to different local yield strengths along the cross-section of the sample. In fact, the local yield strength in the strongly-affected region is increased as a result of strain hardening and grain refinement phenomena, which in turn contribute to larger elastic recovery during unloading [36]. The ratio of h_f/h_{max} can also be correlated to pile-up amount. It was reported that pile-up amount is large when h_f/h_{max} is very close to 1 and the degree of work hardening is small [25, 26]. This observation is consistent with our experimental results. Pile-up phenomenon was investigated in the SMAT-affected region, which will be discussed in detail in Section 3.3.

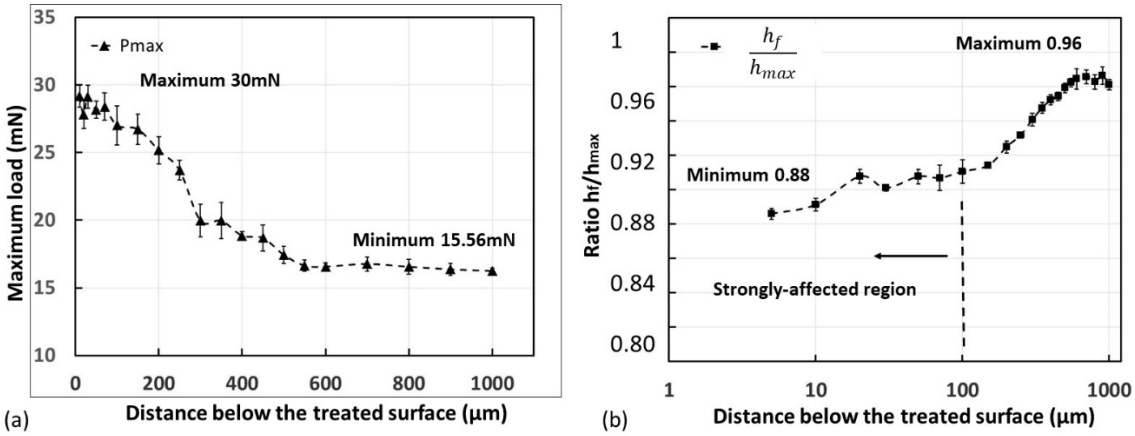

Figure 3 – (a) Maximum loads for indentations performed along the cross-section of the SMAT-processed sample, (b) Corresponding h_f/h_{max} ratios.

The corresponding hardness measured along the cross-section of SMAT-processed and untreated samples is given in Fig. 4. For the SMAT-processed sample, the hardness is the highest in the nanocrystalline region with a value of about 5.06 GPa while this value is about 2.60 GPa for the non-affected bulk of the material. The hardness decreases with the distance along the cross-section and is stabilized at a depth of about 550 µm, which is consistent with the result of the maximum load presented above. For the untreated sample, the hardness is also slightly higher near the sample surface. This could be mainly attributed to the work hardening unintentionally induced during machining. The value of hardness stabilizes at a depth of about 150 µm which could correspond to the depth affected by machining.

Grain refinement effect, compressive residual stress and strain hardening all contribute to higher measured value of hardness. A major challenge would be to distinguish the influence of each factor individually. Note that hardness is calculated by dividing the indentation load by the contact area. On the one hand, it was previously assumed that compressive residual stresses do not have a pronounced effect on the indentation load [26, 31–33]. On the other hand, pile-up phenomenon is detected in the SMAT-affected region, which caused errors in the contact area. In the following section, the pile-up behaviour of SMAT-processed material will first be discussed and the values of hardness will be corrected taking into account the pile-up phenomenon. Then, the corrected hardness will be plotted as a function of the inverse of grain size square root (Hall-Petch law). In the end, a detailed discussion is dedicated to the individual contributions of grain refinement and strain hardening phenomena to higher hardness.

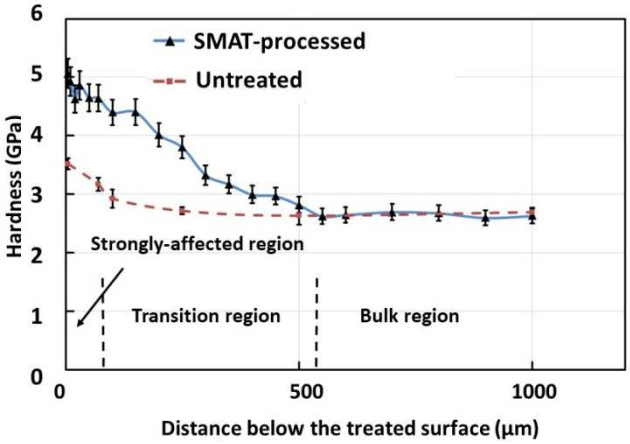

Figure 4 – Hardness measured along the cross-section of SMAT-processed and untreated samples.

3.3 Pile-up behaviour of SMAT-processed material

For an indentation into an elastic material, the surface of the material is typically drawn inwards and downwards underneath the indenter and sinking-in occurs. When the contact involves plastic deformation, the material may either sink in, or pile up around the indenter. This depends on the ratio E/Y (elastic modulus/yield stress) and the strain-hardening properties of the material [25]. For 316L stainless steel usually with a high strain hardening exponent and a high ratio of E/Y, sink-in phenomenon is expected, as illustrated in Fig. 5b in which AFM measurements were performed on an indentation imprint located at 800 µm below the treated surface. For this region far from the treated surface, the local microstructure and mechanical properties were not affected by SMAT. However, for the regions affected by SMAT, the local microstructure and mechanical properties, such as grain size, local yield stress and work hardening exponent [36], change accordingly. As a consequence, pile-up occurred in the SMAT-affected regions, as shown in Fig. 5a for an indentation imprint obtained at 50 µm below the treated surface.

Pile-up behaviour during nanoindentation has been a popular research topic and it can be correlated to material's strain hardening exponent, residual stress states, ratio of E/Y [25, 26, 30, 32, 35, 37]. The main parameter that affects the pile-up behaviour is the strain hardening properties of materials [24, 27, 32]. For materials with low strain-hardening, pile-up tends to occur while for materials that exhibit high strain-hardening (316L stainless steel, for instance), sink-in is expected. Moreover, residual stresses are also reported to have an influence on the pile-up behaviour. In the literature, many studies concluded that compressive residual stress increases the amount of pile-up while tensile residual stress has the opposite effect [25, 31, 32].

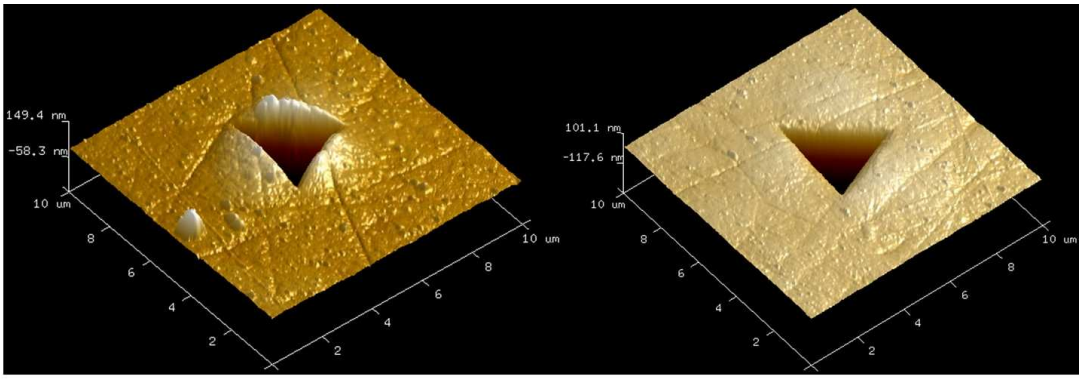

(a) (b)

Figure 5 – AFM measurements of indentation imprints (a) located at 50 µm below the treated surface, (b) located at 800 µm below the treated surface, respectively.

Pile-up behaviour can be quantified by pile-up height [24, 27] or pile-up width [37] depending on the developed method. It is generally accepted that pile-up increases the contact area between the material and the indenter, systematically leading to an erroneous contact area and consequently to an overestimation of the values of hardness and indentation modulus [26, 38]. In this work, a modified model based on the semi-ellipse model of Kese [37] was used in order to evaluate the true contact area affected by pile-up. Fig. 6 gives two examples of AFM 2D data of indentation imprints located at 20 µm and 100 µm below the treated surface respectively. It can be noted that the pile-up shapes and distribution around the three indentation edges are irregular. This phenomenon is different from that observed in the studies presented in the literature [27, 37] where the pile-up behaviour was more regular and was rather evenly distributed along the entire indentation edges. This difference may be attributed to the gradient microstructure generated by SMAT. In the literature, the studied materials often have a fixed average grain size and a given residual stress state throughout the sample. Nevertheless, for the SMAT-processed 316L stainless steel used in this work, a gradient microstructure is generated with a microstructure and mechanical properties varying according to the distance beneath the treated surface. This inhomogeneous microstructure probably leads to irregular pile-up shapes and distribution. In addition, grain orientations were reported to have an influence on the pile-up behaviour [38, 39]. Therefore, the semi-ellipse model of Kese cannot be directly applied for the evaluation of the true contact area in our case of SMAT-processed material.

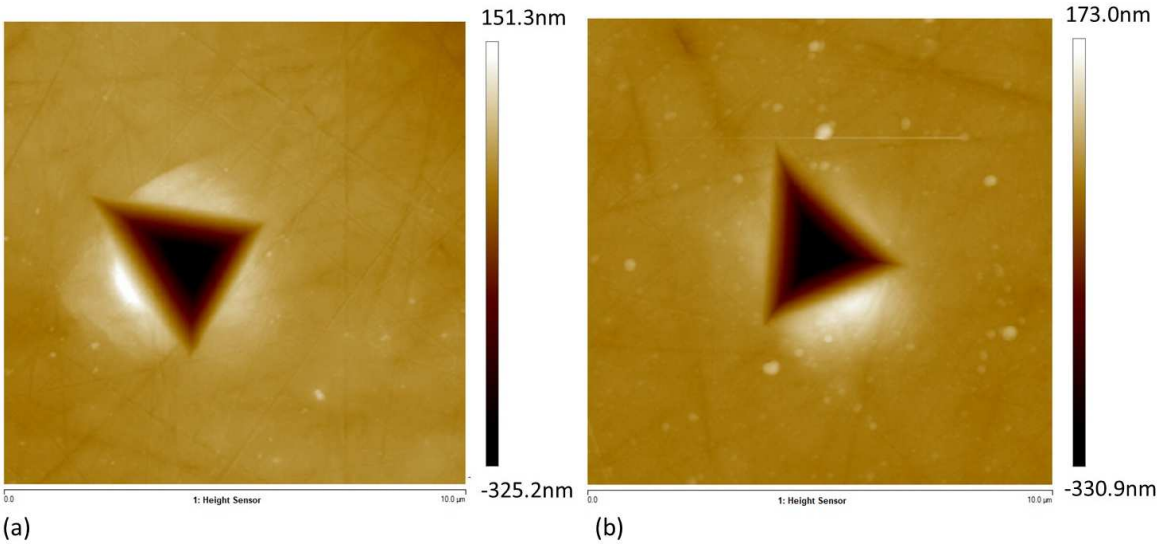

Figure 6 – AFM 2D data of indentation imprints (a) located at 20 µm below the treated surface, and (b) located at 100 µm below the treated surface.

Fig. 7a illustrates the semi-ellipse model of Kese [37] in which the pile-up is assumed to occur along the entire indentation edges. Therefore, the additional increased contact area due to pile-up would be the sum of the three projected areas of pile-up, namely the sum of three semi-ellipses, shown in Fig. 7a. The pile-up length b is considered to be constant and only the pile-up width, a, varies. Nevertheless, in the case of the 316L stainless steel studied in this work, the pile-up shapes and distributions are irregular, leading to varied pile-up length and width. Therefore, the additional increased contact area A_{pu} should be calculated with individual pile-up length and pile-up width measured with AFM, as demonstrated in Fig. 7b. In this work, the pile-up length, width and height (b_i, a_i, h_i where i=1,2,3) for each indentation imprint were measured. It should be mentioned that the indentation pattern is a triangle with three edges. Pile-up parameters (length, width and height) of the three indentation edges were measured simultaneously.

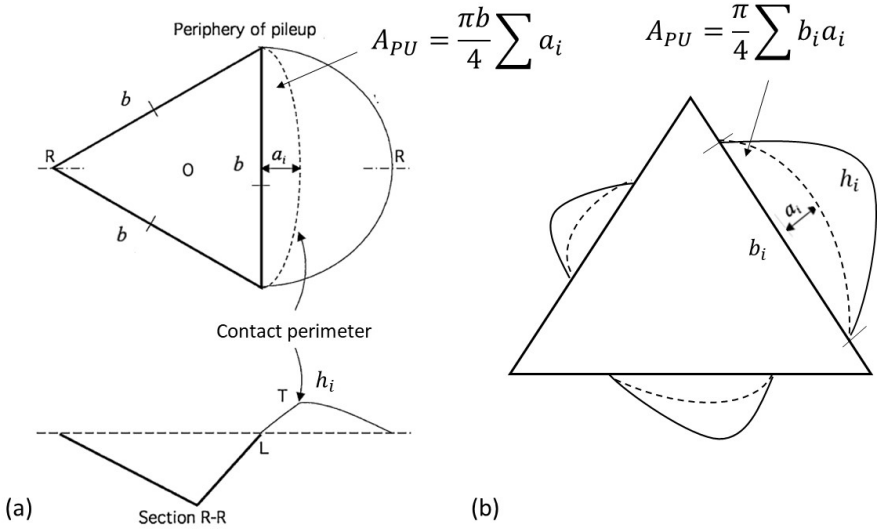

Figure 7 – (a) Ideal semi-elliptical pile-up projected contact area [37], (b) Real pile-up projected contact area of SMAT-processed 316L stainless steel adopted in this work.

While the additional increased contact area due to pile-up can be calculated by pile-up length and width, the pile-up height is another crucial parameter to quantify pile-up behaviour. For our experiments, the pile-up height was measured for the three sides of each triangle indentation imprint and the average value was calculated subsequently. The corresponding results are shown in Fig. 8. It can be observed that the pile-up height is almost constant for indentations located at the near surface region until a depth of 100 µm. It decreases dramatically for indentations located at 300 µm below the treated surface. The pile-up phenomenon seems to disappear at a depth of about 500 µm below the surface. This indicates that the depth affected by SMAT is at least 500 µm, which is consistent with the results of hardness shown above. Higher values of pile-up height for indentations near the treated surface (up to a depth of 100 µm) could be related to the effect of severe grain refinement induced by SMAT according to the previous results of EBSD observations. Moreover, the multilayer macroscopic model of SMAT-processed 316L stainless steel of Petit et al. [36] showed that grain refinement was associated with a decrease in strain hardening exponent and an increase of yield stress. It was previously concluded that strain hardening exponent, n, is a major factor that results in pile-up phenomenon [25, 27, 32]. Severe grain refinement near the treated surface provides the explanation for high values of pile-up height in this region as a consequence of low strain hardening exponent. When the SMAT intensity is low and no significant grain refinement occurs, the strain hardening exponent does not significantly change, which leads to lower value of pile-up height. This is the case of indentation performed at a depth of 300 µm below the treated surface, where a significant decrease of pile-up height value is observed. Another secondary factor that can increase the pile-up height is compressive residual stress according to the literature [24-26, 30-32]. Numerous studies have been dedicated to quantify the influence of residual stress on pile-up height. For instance, Bolshakov et al. [26] used finite element method to study the relation between pile-up height and the residual stress for an 8009 aluminium alloy. It turned out that pile-up value for simulation with a residual stress magnitude of -300 MPa increased by about 20 nm, as compared to stress-free state. The studies of Zhu et al. [24] have led to similar conclusion for a 1045 steel. Pile-up height has also a straightforward link with the indentation load. It was demonstrated that pile-up height increases with increasing indentation load [27]. Gale et al. [27] studied the pile-up behaviour of SMAT-processed copper. The results revealed that pile-up height has a linear relation with indentation load. However, the relation between pile-up height and indentation load is out of the scope of this paper.

The residual stress profile measured along the cross-section of SMAT-processed sample (the same SMAT conditions as our case) presented by Zhou et al. [13] showed that the magnitude of compressive residual stress in the strongly affected region (down to a depth of 150 µm) was in the range of -350 MPa to -450 MPa. Based on the above discussion, the influence of these compressive residual stresses on pile-up height can be qualitatively estimated to be tens of nanometers. Despite the efforts, it is almost impossible to quantify the influence of residual stress in SMAT-processed 316L stainless steel as grain refinement effect and compressive residual stress in the affected region are strongly coupled and both vary according to the distance from the treated surface.

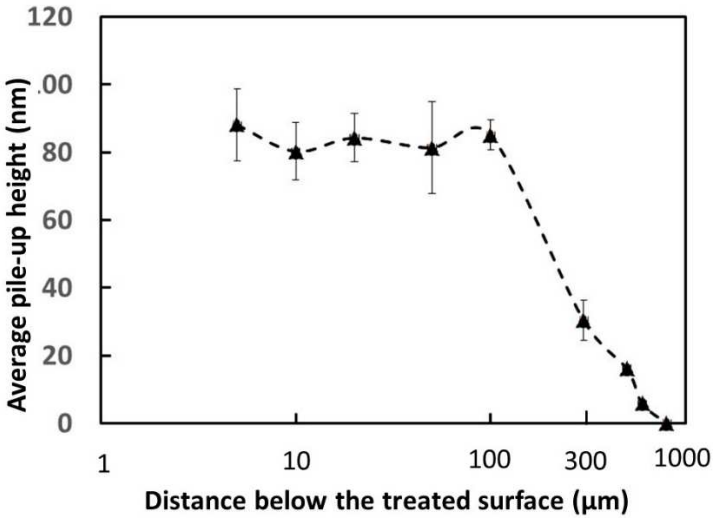

Figure 8 – Average pile-up height for indentations along the cross-section of the SMAT-processed sample.

A modified method based on the semi-ellipse model of Kese [37] was used to evaluate the true contact area using the AFM data (pile-up length and pile-up width), as discussed previously. The corrected true contact area are plotted in comparison with the original one, as shown in Fig. 9a. The corresponding results of hardness before and after correction are also shown in Fig. 9b. With pile-up taken into account, the real contact area should be $A=A_{O-P}+A_{pu}$ where A_{O-P} is the original contact area calculated by standard Oliver-Pharr method and A_{pu} is the sum of the projected areas of three pile-ups around the indentation imprint edges. The new contact area is subsequently used to recalculate the hardness. A decrease in hardness can be observed (Fig. 9b). For instance, the original hardness for the nanocrystalline region is about 5.03 GPa while this value is decreased to 4.20 GPa when corrected with the new contact area. It should be stressed out that several methods exist to account for the true contact area in the case of pile-up [24, 25, 27, 37], but each method is restricted to a specific studied material or to a certain loading range. It is possible that our modified method might not precisely quantify the irregular pile-up amount. It will therefore be interesting to find a method to more accurately correct pile-ups for SMAT-processed materials in future work. Although it was generally concluded in the literature that pile-up correction is necessary for the sake of accuracy [24, 25, 27, 37], the necessity of its correction might be questioned by some. For instance, the pile-up formation around the indenter tip may not bear the load the way a material beneath the free surface would bear.

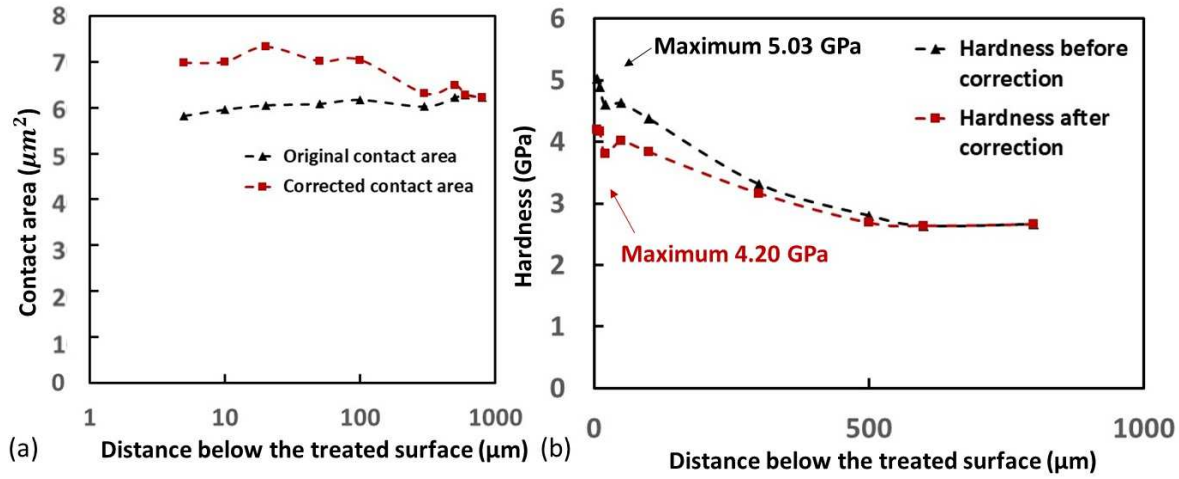

Figure 9 – (a) Original contact area using standard Oliver-Pharr method compared to corrected contact area using a modified method, (b) Corresponding hardness results before and after correction.

In Section 3.1, the distribution of grain size along the cross-section of SMAT-processed sample is highlighted according to EBSD observations. It could be concluded that grain refinement is severe down to a depth of about 100 µm. The evolution of the hardness values (before and after correction) at depths between 5 and 100 µm below the treated surface according to the inverse of the square root grain size ($\sqrt{d}^{-1}$) is shown in Fig. 10. The corresponding Hall-Petch coefficient K for the corrected hardness can then be determined and is about 251.5 $MPa * \mu m^{1/2}$. Experimentally, the value of K could vary depending on several factors such as strain levels, temperature and history/preparation of the sample [40, 41]. To be able to compare the results of this study with those of the literature, it is important to note that the strain distribution under a pyramidal indenter is not uniformed. The concept of representative strain, ε_r, gives an overall estimation of the average strain level during a nanoindentation test. Tabor [41] estimated theoretically and experimentally that this value is about 8% for Vickers indenter. This value was extended to Berkovich tip. Kashyap et al. [42] investigated the Hall-Petch coefficient K of tensile specimens of 316L stainless steel (grain size: 3.1 µm to 86.7 µm) at different strain levels and temperatures. Their results showed that the value of the K coefficient at room temperature (24°C) and at a 8% strain level was about 280 $MPa * \mu m^{1/2}$, which is very close to the value obtained in this work. This may indicate that the corrected hardness agrees well with the Hall-Petch law and that grain refinement effect could be the major factor that leads to higher local strength for SMAT-processed materials. On the basis of this conclusion, the contribution of strain hardening to the local yield strength can be assumed less significant in an indirect manner. This is mainly due to the fact that strain hardening is difficult to be individually and quantitatively characterized by experimental methods [43].

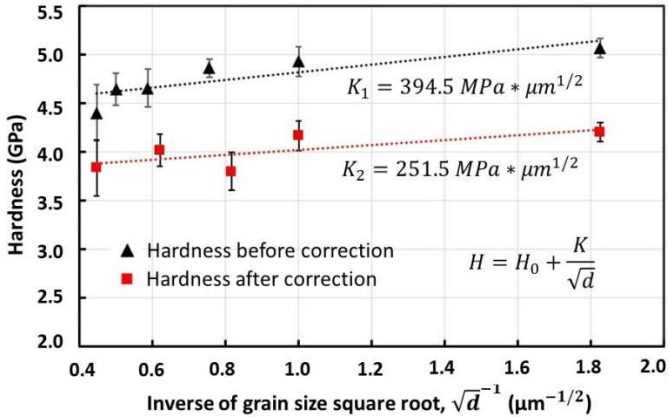

Figure 10 – Hardness values before and after pile-up correction plotted as function of the inverse of grain size square root.

4. Conclusion

In this work, the mechanical properties at different depths in the gradient microstructure of a 316L stainless steel generated by SMAT were studied with nanoindentation technique. The results of indentation tests were analysed by combining the observation of microstructure using EBSD and that of indentation imprint using AFM. The following conclusions can be drawn:

1) EBSD observation revealed that the thickness of the well formed nanostructured layer is about 5 µm and the corresponding grain size in this layer ranges from 50 to 300 nm. Grain refinement effect is severe within a depth around 100 µm beneath the treated surface.
2) Grain refinement seems to be the major factor that results in higher hardness in the strongly-affected region.
3) Severe grain refinement in the near treated surface is associated with a decrease in strain hardening exponent. Pile-up phenomenon is observed in the SMAT-affected region due to low strain hardening exponent. A modified model was applied to evaluate the nanoindentation true contact area by taking into account pile-up phenomenon. The values of hardness recalculated with corrected contact area were found to slightly decrease.

Acknowledgements

Financial support from the University of Technology of Troyes, Grand Troyes and Conseil Départemental de l'Aube through CompNano project is greatly appreciated. Thierry Baudin and his team are acknowledged for EBSD observations. Z. Sun acknowledges the University of Technology of Troyes for the funding of his Tenure-Track position. Y. Wu would like to express his cordial gratitude to the Chinese Scholarship Council (CSC) for the financial support of his PhD scholarship in France.

References

[1] M.A.S. Torres, H.J.C. Voorwald, International Journal of Fatigue, 24 (2002) 877–886.

[2] E.R. de los Rios, A. Walley, M.T. Milan, G. Hammersley, International Journal of Fatigue, 17 (1995) 493–499.

[3] R.K. Nalla, I. Altenberger, U. Noster, G. Liu, Materials Science and Engineering A, 355 (2003) 216–230.

[4] W. Zhuang, Q. Liu, R. Djugum, P.K. Sharp, A. Paradowska, Applied Surface Science, 320 (2014) 558–562.

[5] G. Kermouche, G. Pacquaut, C. Langlade, J.M. Bergheau, Compte-Rendu Mécanique, 339 (2011) 552–562.

[6] H. Zhang, Z. Hei, G. Liu, J. Lu, K. Lu, Acta Materialia, 51 (2003) 1871–1881.

[7] J. Uusitalo, L.P. Karjalainen, D. Retraint, M. Palosaari, Materials Science Forum, 604–605 (2009) 239–248.

[8] N.R. Tao, Z.B. Wang, W.P. Tong, M.L. Sui, J. Lu, K. Lu, Acta Mater, 50 (2002) 4603–4616.

[9] K. Lu, J. Lu, Materials Science and Engineering A, 375–377 (2004) 38–45.

[10] Y. Samih, B. Beausir, B. Bolle, T. Grosdidier, Materials Characterization, 83 (2013) 129–138.

[11] G. Proust, D. Retraint, M. Chemkhi, A. Roos, C. Demangel, Microscopy and Microanalysis, 21(4) (2015) 919–926.

[12] Z. Sun, D. Retraint, T. Baudin, A.L. Helbert, F. Brisset, M. Chemkhi, J. Zhou, P. Kanouté, Materials Characterization, 124 (2017) 117–121.

[13] J. Zhou, Z. Sun, P. Kanouté, D. Retraint, International Journal of Fatigue, 103 (2017) 309–317.

[14] G. Proust, P. Trimby, S. Piazolo, D. Retraint, J. Vis. Exp., 122 (2017) 1–7.

[15] T. Roland, D. Retraint, K. Lu, J. Lu, Materials Science and Engineering A, (2007) 445–446, 281–288.

[16] M.F. Doerner, W.D. Nix, Critical Reviews in Solid State and Materials Sciences, 14 (1988) 225–268.

[17] W.D. Nix, Materials Science and Engineering A, 234–236 (1997) 37–44.

[18] D. Chicot, M. Yetna N'Jock, E.S. Puchi-Cabrera, A. Iost, M.H. Staia, G. Louis, G. Bouscarrat, R. Aumaitre, Thin Solid Films, 558 (2014) 259–266.

[19] T. Pardoen, Journal of The Mechanics and Physics of Solids, 62 (2014) 81–98.

[20] D. Mercier, V. Mandrillon, G. Parry, M. Verdier, R. Estevez, Thin Solid Films, 638 (2017) 34–47.

[21] Y. Choi, W.Y. Choo, D. Kwon, Scripta Materialia, 45 (2001) 1401–1406.

[22] H.U. Rehman, K. Durst, S. Neumeier, A.B. Parsa, A. Kostka, G. Eggeler, M. Göken, Materials Science & Engineering A, 634 (2015) 202–208.

[23] G. Cheng, K.S. Choi, X. Hu, X. Sun, Materials Science & Engineering A, 652 (2016) 384–395.

[24] L.N. Zhu, B.S., Xu, H.D. Wang, C.B. Wang, Materials Characterization, 61(12), (2010) 1359–1362.

[25] L.N. Zhu, B.S., Xu, H.D. Wang, C.B. Wang, Critical Reviews in Solid State and Materials Sciences, 40(2), (2015) 77–89.

[26] A. Bolshakov, W.C. Oliver, G.M. Pharr, Journal of Materials Research, 11(03), (1996) 760–768.

[27] J.D. Gale, A. Achuthan, Journal of Materials Science, 49(14), (2014) 5066–5075.

[28] P. Juran, P.J. Liotier, C. Maurice, F. Valiorgue, G. Kermouche, Comptes Rendus - Mécanique, 343 (5–6), (2015) 344–353.

[29] Z.H. Xu, X. Li, Philosophical Magazine, 86(19), (2006) 2835–2846.

[30] M.K. Khan, M.E. Fitzpatrick, S.V. Hainsworth, L. Edwards, Computational Materials Science, 50(10), (2011) 2967–2976.

[31] L.N. Zhu, B.S., Xu, H.D. Wang, C.B. Wang, Materials Chemistry and Physics, 136(2–3), (2012) 561–565.

[32] C.E.K. Mady, S.A. Rodriguez, A.G. Gómez, R.M. Souza, Surface and Coatings Technology, 205(5), (2010) 1393–1397.

[33] P.J.J. Withers, H.K.D.H. Bhadeshia, Materials Science and Technology, 17(4), (2001) 355–365.

[34] W.C. Oliver, G.M. Pharr, J. Mater. Res. 7 (1992) 1564–1583.

[35] A.E. Giannakopoulos, S. Suresh, Scripta Materialia, 40(10), (1999) 1191–1198.

[36] J. Petit, L. Waltz, G. Montay, D. Retraint, A. Roos, M. François, Materials Science and Engineering A, 536, (2012) 124–128.

[37] K.O. Kese, Z.C. Li, B. Bergman, Materials Science and Engineering A, 404(1–2), (2005) 1–8.

[38] E. Renner, Y. Gaillard, F. Richard, F. Amiot, P. Delobelle, International Journal of Plasticity, 77, (2016) 118–140.

[39] Y. Wang, D. Raabe, C. Klüber, F. Roters, Acta Materialia, 52(8), (2004) 2229–2238.

[40] Z.C. Cordero, B.E. Knight, C.A. Schuh, International Materials Reviews, 61(8), (2016) 495–512.

[41] D. Tabor, The Hardness of Metals, Clarendon Press, Oxford, 1951.

[42] B.P. Kashyap, K. Tangri, Acta Metallurgica et Materialia, 43(11), (1995) 3971–3981.

[43] J. Zhou, Z. Sun, P. Kanouté, D. Retraint, Mechanics of Materials, 127, (2018), 100–111.

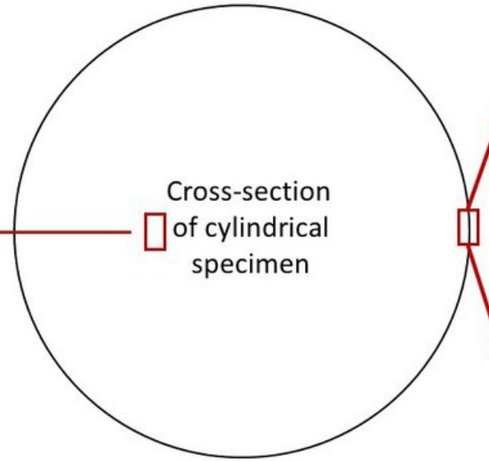

Treated surface

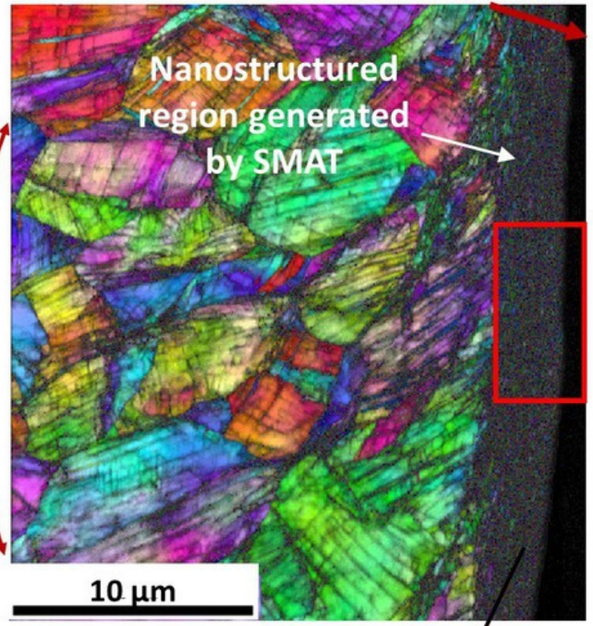

Nanoindentation imprint in the bulk region

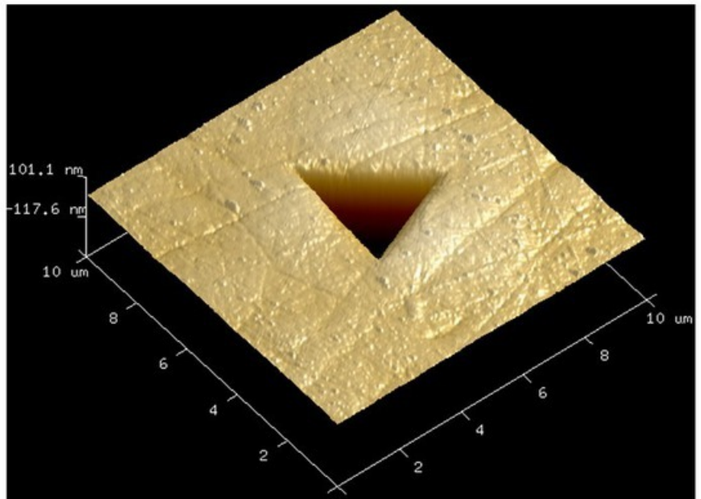

Nanoindentation imprint in the nanostructured region

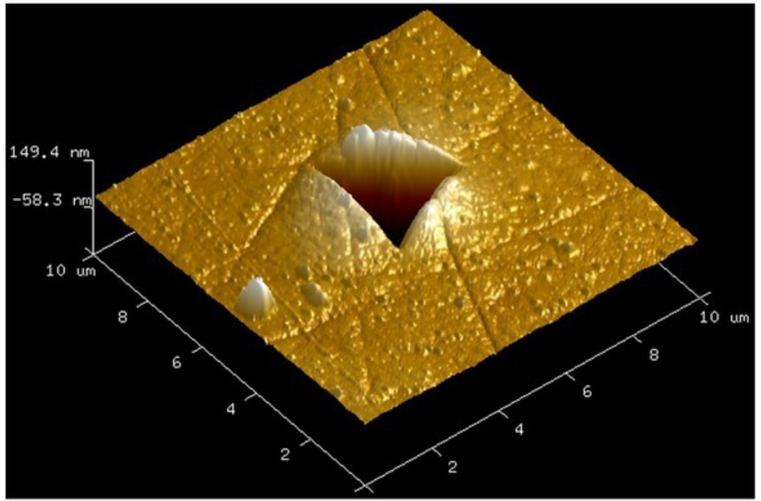

Correction of true contact area due to pile-up

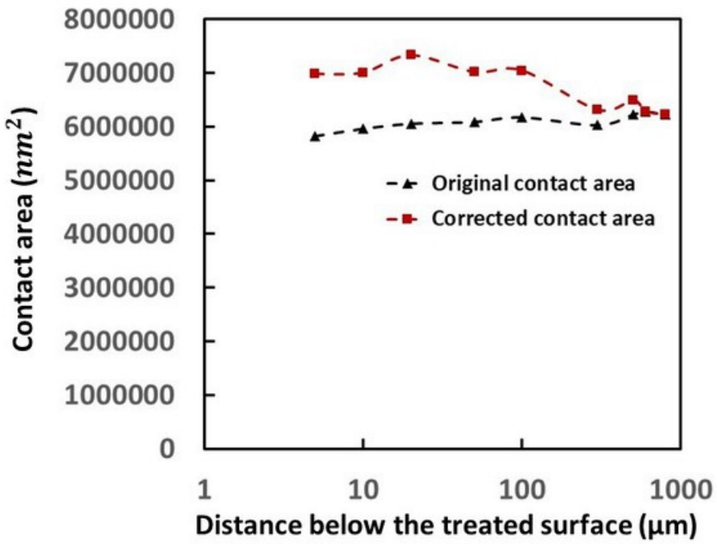

Correction of hardness due to pile-up